Earth and Planetary Science Letters 479 (2017) 377–386

Contents lists available at ScienceDirect

Earth and Planetary Science Letters

www.elsevier.com/locate/epsl

The duration of a Yellowstone super-eruption cycle and implications for the age of the Olduvai subchron

Tiffany A. Rivera [a,*], Rachel Darata [a], Peter C. Lippert [b], Brian R. Jicha [c], Mark D. Schmitz [d]

[a] Westminster College, 1840 S 1300 E, Salt Lake City, UT 84105, United States
[b] The University of Utah, 115 S 1460 E, Salt Lake City, UT 84112, United States
[c] University of Wisconsin-Madison, 1215 West Dayton St., Madison, WI 53706, United States
[d] Boise State University, 1910 University Drive, Boise, ID 83725, United States

ARTICLE INFO

Article history:
Received 28 April 2017
Received in revised form 18 August 2017
Accepted 21 August 2017
Available online 28 September 2017
Editor: T.A. Mather

Keywords:
geomagnetic polarity time scale
$^{40}Ar/^{39}Ar$
geochronology
paleomagnetism
super-eruptions
magma recharge

ABSTRACT

Small-volume rhyolitic eruptions preceding and following a caldera-forming eruption can provide insights into the tempo of eruption cycles and timing of magmatic recharge. In this contribution, high-precision $^{40}Ar/^{39}Ar$ eruption ages were obtained on the three effusive eruptions bracketing the Huckleberry Ridge Tuff, which comprise Yellowstone's first volcanic cycle. These dates are supplemented with detailed paleomagnetic and rock magnetic analyses to resolve discrepancies with previous reported stratigraphy. The Huckleberry Ridge Tuff (2.08 Ma) was preceded by an eruption at 2.14 Ma, and followed by eruptions at 1.98 and 1.95 Ma, all of which occurred during four distinct periods of geomagnetic instability within the Matuyama chron. The first volcanic cycle of Yellowstone has now been constrained to within a 200 kyr timespan, or half of the previously proposed duration, and similar to the duration of volcanic activity for caldera-forming systems in the Jemez Volcanic Field. The maximum duration for magmatic recharge for the first Yellowstone volcanic cycle is no greater than 100 kyr, and likely closer to 40 kyr. Furthermore, the combined $^{40}Ar/^{39}Ar$ eruption ages and paleomagnetic results provide polarity anchors for the Pre-Olduvai excursion and Olduvai subchron, which are often used as tie-points in studies of early Pleistocene hominin evolution.

1. Introduction

Recent developments in analytical capabilities have significantly improved the accuracy and precision of eruption ages for volcanic events. In particular, the precision of $^{40}Ar/^{39}Ar$ dates can now reach well below ±1%, thus permitting fine-scale resolution of eruption stratigraphy, especially for the Quaternary. Recently, this high-precision dating technique, along with zircon U–Pb dating, has been applied to the eruptive stratigraphy within the Yellowstone Volcanic Field in order to refine eruption ages for the three caldera-forming eruptions. These efforts have resulted in an eruption age of 2.077 ± 0.004 Ma (0.24%) for the Huckleberry Ridge Tuff (Rivera et al., 2014; Singer et al., 2014), 1.300 ± 0.001 Ma (0.08%) for the Mesa Falls Tuff (Rivera et al., 2016; Ellis et al., 2017), and 0.631 ± 0.004 Ma (0.6%) for the Lava Creek Tuff (Matthews et al., 2015; Rivera and Jicha, 2015; Jicha et al., 2016).

While the eruptions that have generated the calderas of the Yellowstone Volcanic Field have been widely studied, numerous rhyolite domes and lava flows erupted between caldera-forming events have received less attention towards understanding magmatic processes in the region. Early work in the region led Christiansen et al. (1972) to separate the volcanism into three cycles, with each cycle containing one of the major ash-flow sheets mentioned above, along with pre- and post-caldera effusive basalts and rhyolites. Recent work on smaller-volume eruptions from each of these cycles has led to increased understanding of magmatic generation durations and processes, as well as identifying periods of magmatic quiescence between eruptions (Bindeman and Simakin, 2014; Bindeman et al., 2008; Rivera et al., 2014; Troch et al., 2017; Wotzlaw et al., 2015). Thus, improved knowledge of these effusive units in terms of their age, distribution, and chemistry will assist in a broader understanding of the unique tectonic and magmatic setting of the Yellowstone Volcanic Field.

Between the caldera-forming eruptions that produced the Huckleberry Ridge and Mesa Falls Tuffs, a series of four to six smaller volume rhyolitic eruptions surfaced. The earliest two, the Headquarters and Blue Creek Flows, along with the pre-caldera Rhyolite of Snake River Butte, were grouped as "first-cycle" erup-

* Corresponding author.
E-mail address: trivera@westminstercollege.edu (T.A. Rivera).

http://dx.doi.org/10.1016/j.epsl.2017.08.027
0012-821X/

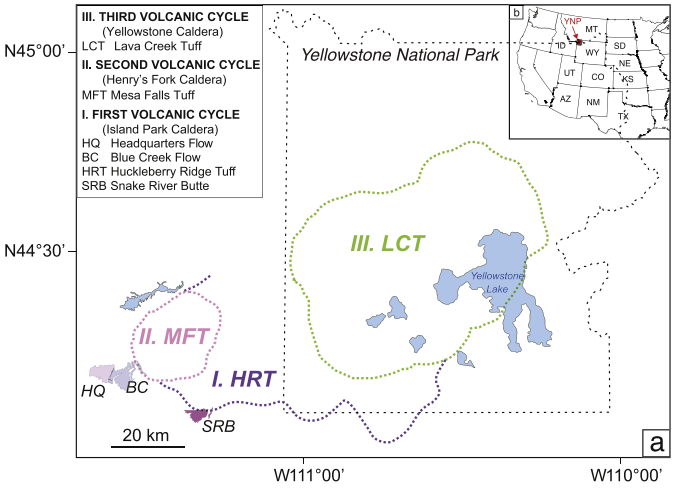

Fig. 1. (a) Location map of the Yellowstone Volcanic Field calderas and the mapped extent of the Headquarters Flow (HQ), Blue Creek Flow (BC), and Rhyolite of Snake River Butte (SRB). Base map modified from Troch et al. (2017). (b) Location of Yellowstone National Park within the United States of America.

tions based on whole rock chemical analyses similar to the Huckleberry Ridge Tuff (Christiansen, 1982, 2001). These flows were estimated to erupt at ca. 1.8–2.0 Ma using imprecise (±3% uncertainties) K/Ar sanidine dating (Obradovich, 1992). Initial paleomagnetic investigations revealed that all of these rhyolites preserved a normal polarity direction (Christiansen, 1982), distinct from the transitional polarity preserved by the Huckleberry Ridge Tuff and the reversed polarity preserved by the Mesa Falls Tuff (Reynolds, 1977). Combining the polarity and K/Ar dates suggests that the younger eruptions occurred during the Olduvai normal polarity subchron, whereas the older Rhyolite of Snake River Butte erupted during the Reunion subchron, with a total first-cycle duration spanning some 400 kyr (Obradovich, 1992). The first cycle coincides with a period of geomagnetic instability within the Matuyama chron that has been widely discussed and investigated (e.g., Channell et al., 2002, 2003, 2016; Singer, 2014; Singer et al., 2014; among others). Given that the geomagnetic polarity time scale is used in a variety of geochronologic applications, including marine sediment correlation for understanding climatic changes and archaeological investigations to provide maximum or minimum ages on events in human evolution, it is important to provide accurate and precise anchors for geomagnetic polarity events.

This contribution provides new high precision $^{40}Ar/^{39}Ar$ eruption ages for the Rhyolite of Snake River Butte, the Blue Creek Flow, and the Headquarters Flow. We supplement our ages with detailed paleomagnetic and rock magnetic analyses to re-evaluate the earlier assignment of the two younger flows to the Olduvai normal polarity subchron. Our results provide anchors for the geomagnetic polarity time scale, constrain periods of volcanic quiescence, and address the longevity of the first eruption cycle of the Yellowstone Volcanic Field.

2. Materials and methods

2.1. Sample locations and descriptions

The Headquarters and Blue Creek Flows were sampled west of Big Bend Ridge (Fig. 1), interpreted as the shared rim of the Island Park and Henry's Fork calderas. Sampling coordinates are provided in Table 1. Both lava flows have a weathered exterior, with a white devitrified interior matrix and phenocrysts of plagioclase, sanidine, and quartz up to 3 mm readily apparent. Phenocrysts are generally colorless and translucent, however, some grains have altered to a pale yellow–orange color. In thin section, grains of fayalite are also found (Fig. 2).

The Rhyolite of Snake River Butte was sampled near the top of the lava dome, along the easternmost edge of Big Bend Ridge. This sample corresponds to that analyzed by Rivera et al. (2014). While fresher than samples of Blue Creek and Headquarters Flows, the Rhyolite of Snake River Butte is characterized by a white, devitrified groundmass and a similar phenocryst assemblage of sanidine, plagioclase, and quartz (Fig. 2). This lava represents the earliest known rhyolitic eruption of the Yellowstone Volcanic Field as it directly underlies the Huckleberry Ridge Tuff (Christiansen, 1982). Existing K/Ar sanidine dates place eruption at about 2.0 Ma; however this defies the stratigraphic order with respect to the new high-precision $^{40}Ar/^{39}Ar$ eruption age of the Huckleberry Ridge Tuff. Recent work on zircon crystals extracted from the Rhyolite of Snake River Butte has suggested zircon crystallization from 2.2 to 2.15 Ma (Rivera et al., 2014; Wotzlaw et al., 2015). While these zircon crystallization ages suggest resolution of the stratigraphic relationship between the Rhyolite of Snake River Butte and the Huckleberry Ridge Tuff, they do not necessarily constrain the eruption age, thus leaving uncertainty in the recurrence interval between this precursory flow and the caldera-forming eruption.

Christiansen (1982) notes that field relationships require the Headquarters Flow to be younger than the Blue Creek Flow. Previously determined K/Ar sanidine dates for these two flows are provided in Table 1. Existing K/Ar ages for these two flows place them in reverse stratigraphic order, however, which Obradovich (1992) recognized. Obradovich (1992) states that these ages may be too young based on potentially incomplete degassing of the sanidine crystals. Christiansen (1982) assigned a normal polarity direction to both flows although analytical methods and data for the paleomagnetic results were never published.

2.2. $^{40}Ar/^{39}Ar$ feldspar age determinations

Feldspars were separated from the bulk rock and handpicked for analysis using a binocular microscope. Grains ranging from 1–3 mm were loaded into an aluminum disk along with the Alder Creek Rhyolite sanidine neutron fluence monitor and irradiated in the cadmium-lined in-core irradiation tube (CLICIT) at the Oregon State University TRIGA reactor. Argon analyses were performed at the University of Wisconsin-Madison using a 60 W CO_2 laser and a Nu Instruments Noblesse multi-collector mass spectrometer. Monitor analyses were performed as single crystal fusions, whereas single feldspars from the Snake River Butte, Headquarters, and Blue Creek Flows were incrementally heated. Analyses of unknowns, monitors, and blanks were carried out in identical fashion. Full analytical methods are provided in Jicha et al. (2016).

We adopt the age of 1.1864 ± 0.0012 Ma (Rivera et al., 2013; Jicha et al., 2016) for the Alder Creek Rhyolite sanidine monitor. We chose 1.1864 Ma because it has been calibrated to the Fish Canyon Tuff sanidine value of 28.201 Ma (Kuiper et al., 2008) and the ^{40}K decay constant (λ) of Min et al. (2000). This calibration is necessary in order to compare with the time scale boundaries presented in the 2012 version of the Geologic Time Scale (Gradstein et al., 2012). All $^{40}Ar/^{39}Ar$ ages are reported with 2σ uncertainty including uncertainties on the irradiation parameter (J) and the ^{40}K decay constant (Min et al., 2000) unless otherwise noted. Full analytical data are provided in the Supplementary Materials, thus allowing for recalculation to other monitor age and decay constant calibrations.

2.3. Paleomagnetic methods

Six to eight 2.5 cm diameter cores were collected for paleomagnetic analyses. Samples were collected with a gasoline powered

Table 1
Sample locations and data types for rhyolitic lavas of Yellowstone's first volcanic cycle. K/Ar sanidine dates of Obradovich (1992) provided with 1σ uncertainty.

Unit	K/Ar date (Obradovich, 1992)	Polarity (Christiansen, 1982)	Latitude (N)	Longitude (E)	Sample	Data type
Blue Creek Flow	1.75 ± 0.04	N	44°12.036′	−111°34.644′	15BCF-1	Ar dates
	1.78 ± 0.03				16BCF-2	6 drill cores
Headquarters Flow	1.86 ± 0.06	N	44°12.831′	−111°38.765′	15HQF-1	Ar dates
	1.78 ± 0.04				16HQF-2	8 drill cores
	1.81 ± 0.04					
Rhyolite of Snake River Butte	1.99 ± 0.04	N	44°08.014′	−111°20.879′	13SRB-1	Ar dates

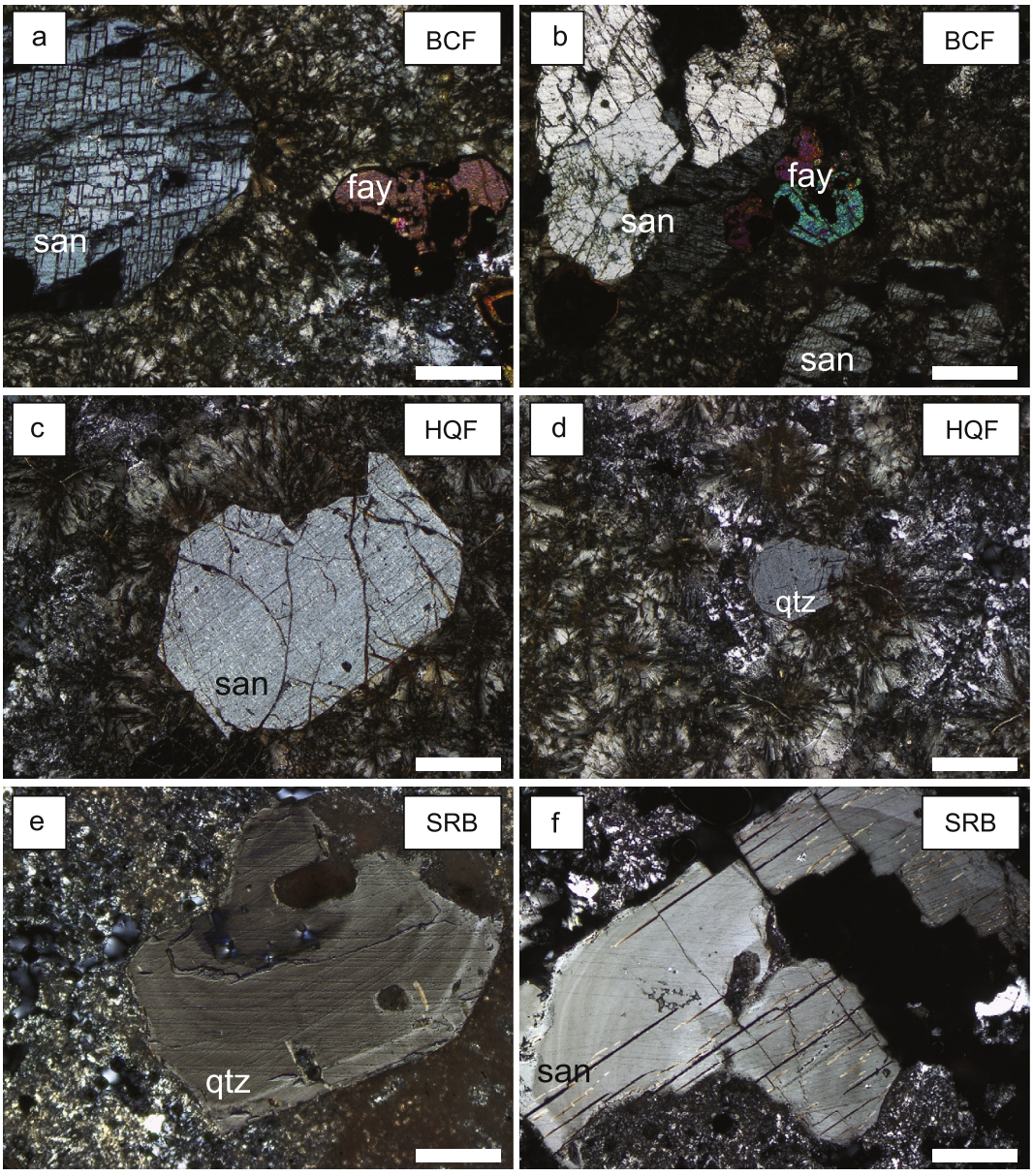

Fig. 2. Photomicrographs of (a–b) Blue Creek Flow (BCF); (c–d) Headquarters Flow (HQF); and (e–f) Rhyolite of Snake River Butte (SRB). All images taken with crossed-polarized light. Scale bar measures 500 μm. Phases indicated are: sanidine (san); fayalite (fay); quartz (qtz). Note spherulitic texture in the groundmass of both BCF and HQF, and zoning preserved in phenocrysts of SRB.

drill over at least one meter of vertical outcrop and several meters of lateral outcrop. All cores were oriented *in situ* with both magnetic and sun compasses. In the absence of field observations to suggest otherwise, we assume that all units have remained untilted since their emplacement.

Paleomagnetic and rock magnetic analyses were conducted at the Utah Paleomagnetic Center at the University of Utah. The natural remanent magnetization (NRM) of each 1.5 to 2.0 cm-long specimen was measured with an AGICO JR-6A spinner magnetometer operating in the fast, six-position automatic mode. The NRM was demagnetized using alternating fields (AF) using a 2G Enterprises single-axis AF demagnetizer. AF demagnetization consisted of at least 14 steps from 2.5 to 140 mT.

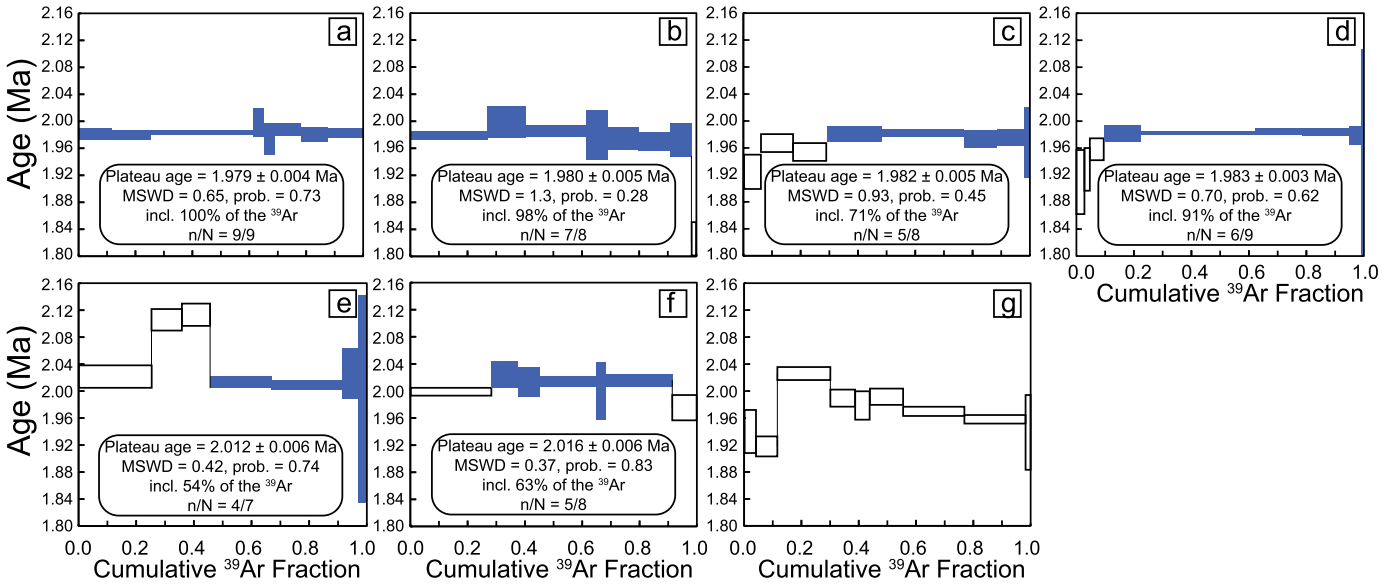

Fig. 3. (a–f) Plateau diagrams for each single feldspar crystal analyzed from the Blue Creek Flow. Steps that define a plateau are indicated by closed boxes; steps excluded from the plateau are shown by open boxes. Box heights include 2σ uncertainty. All plateaus contain more than 50% of the total ^{39}Ar released from the sample (Fleck et al., 1977). (g) Additional grain analyzed that did not yield a plateau. n/N: number of plateau steps (n) of total steps (N) used to calculate the plateau age.

The weak-field temperature dependent magnetic susceptibility (κ–T) of representative specimens was measured using an AGICO MFK1-A Kappabridge in conjunction with its CS4 furnace apparatus. Fresh rock chips were powdered in a ceramic mortar and pestle and approximately 250 mg of material were heated from 20 °C to a peak temperature of 700 °C and returned to 40 °C over the course of two hours; all measurements were completed in argon gas. Raw measurement data were corrected for the κ–T effect of the sample holder and then mass normalized.

Room-temperature magnetic hysteresis curves and isothermal backfield curves for representative specimen chips (~60 mg each) were measured with a LakeShore Cryotronics/PMC MicroMag™ 3900-4 vibrating sample magnetometer (VSM). For the hysteresis loops, specimens were saturated in 1 T, with magnetization measured every 2.5 mT with an averaging time of 100 ms; saturation magnetization (M_s), saturation remanence (M_{rs}), and bulk coercivity (H_c) were calculated after removing the paramagnetic effect of the sample holder and mass normalizing the raw data. Isothermal backfield curves were measured on the same specimen chips immediately following the measurement of the hysteresis loops.

3. Results

3.1. $^{40}Ar/^{39}Ar$ feldspar geochronology

Six of seven single feldspar crystals produced plateaus for sample 15BCF-1 with ages ranging from 1.9793 ± 0.0037 Ma to 2.0160 ± 0.0061 Ma. Four of these grains yield a weighted mean age of 1.9811 ± 0.0020/0.0035 Ma (2σ including J/λ; Mean Square Weighted Deviates (MSWD) = 0.65; $p = 0.74$). Two grains are statistically older (~2.01 Ma). Plateau diagrams for each of the step-heating experiments are provided in Fig. 3.

Plateaus were achieved for four of five analyzed 15HQF-1 feldspar crystals with each plateau including ≥50% of the ^{39}Ar. Plateau ages range from 1.9459±0.0056 Ma to 1.9494±0.0060 Ma, with a weighted mean age of 1.9476 ± 0.0024/0.0037 Ma (2σ including J/λ; MSWD = 0.26; $p = 0.94$). Results for each experiment are provided in Fig. 4.

Each of six incrementally heated single sanidine crystals of sample 13SRB-1 produced a plateau with greater than 75% of the ^{39}Ar. Plateau ages span from 2.1371 ± 0.0036 Ma to 2.1521 ± 0.0043 Ma. A weighted mean age of 2.1398 ± 0.0017/0.0035 Ma (2σ including J/λ; MSWD = 1.51; $p = 0.30$) was calculated for five of the six analyses. Results for each experiment are provided in Fig. 5.

All of our plateaus meet the widely accepted criteria of Fleck et al. (1977), who suggested that a plateau is part of an age spectrum composed of contiguous gas fractions that together represent more than 50% of the total ^{39}Ar released from the sample for which no difference in age can be detected between any two fractions at the 95% confidence level. Blank-corrected raw data for all analyses are provided in the supplemental materials.

3.2. Rock magnetism results

Hysteresis ratios for both the Blue Creek and Headquarters Flows suggest that the predominant remanence carrier is pseudo-single domain (PSD) titanium-poor magnetite (Fig. 6a; Day et al., 1977; Dunlop, 2002). Specimens from both sites plot along a mixing curve between multidomain (MD) magnetite and cubic single domain (CSD) magnetite (Dunlop, 2002); these mixing curves suggest that the Blue Creek Flow contains a large fraction (10–30%) of CSD magnetite grains, whereas the Headquarters Flow has a lower fraction (10%) of these grains. These magnetic hysteresis data are consistent with a population of CSD grains rapidly frozen in volcanic glass (Gee and Kent, 1995) and larger PSD and MD grains distributed in the (relatively) more slowly cooled matrix. This interpretation agrees with the relatively simple Ar plateau diagrams described above. Moreover, the larger fraction of easily remagnetized MD grains in the Headquarters Flow could explain why specimens from this site exhibit stronger viscous magnetic overprints than those from the Blue Creek Flow (see next section).

A squareness plot (Wang and Van der Voo, 2004) of the magnetic hysteresis data for these two lava flows shows that both lavas contain titanium-poor magnetite (Fig. 6b), which is a stable remanence carrier with a high unblocking temperature. While the Day plot emphasizes magnetic grain size heterogeneity, the squareness plot suggests that a non-zero fraction of single domain magnetite is present and is compositionally uniform.

Low-field magnetic susceptibility versus temperature measurements (κ–T) for specimens from both flows show similar characteristics. Heating curves display large and sharp decreases in mag-

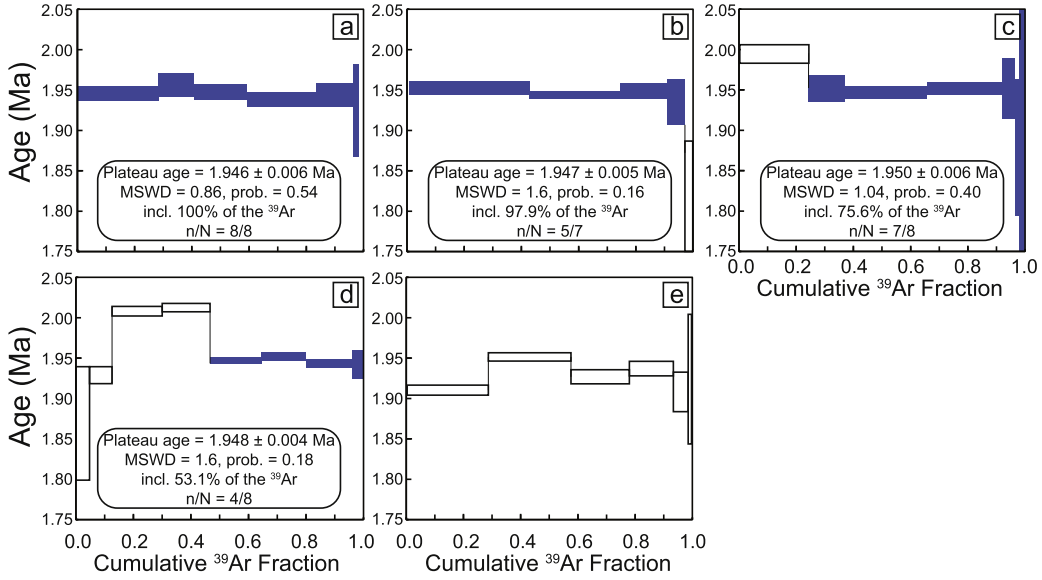

Fig. 4. (a–d) Plateau diagrams for each single feldspar crystal analyzed from the Headquarters Flow. Steps that define a plateau are indicated by closed boxes; steps excluded from the plateau are shown by open boxes. Box heights include 2σ uncertainty. All plateaus contain more than 50% of the total ^{39}Ar released from the sample (Fleck et al., 1977). (e) Additional grain analyzed that did not yield a plateau. n/N: number of plateau steps (n) of total steps (N) used to calculate the plateau age.

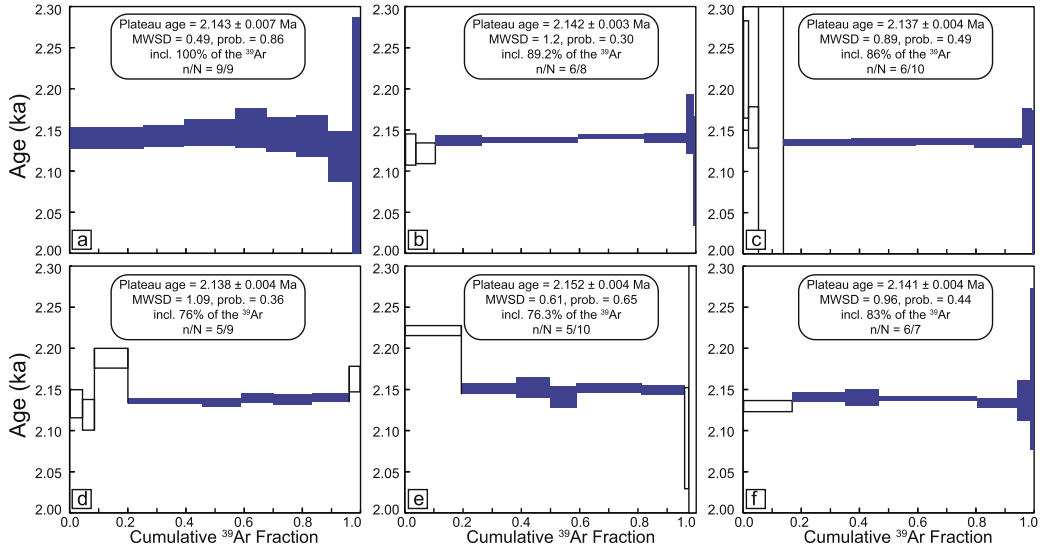

Fig. 5. (a–f) Plateau diagrams for each single feldspar crystal analyzed from the Rhyolite of Snake River Butte. Steps that define a plateau are indicated by closed boxes; steps excluded from the plateau are shown by open boxes. Box heights include 2σ uncertainty. n/N: number of plateau steps (n) of total steps (N) used to calculate the plateau age. All plateaus contain more than 50% of the total ^{39}Ar released from the sample (Fleck et al., 1977).

netic susceptibility between 560–580 °C, while cooling curves exhibit distinctive changes in susceptibility of lower magnitude and at temperatures approximately 10–20 °C lower (Figs. 6c and 6d). The heating curves record the presence of low-Ti titanomagnetite, consistent with inferences from the magnetic hysteresis data described above. In summary, our rock magnetic analyses indicate that both the Blue Creek and Headquarters Flows have a magnetic mineralogy that is capable of and expected to carry a stable magnetic remanence.

3.3. Paleomagnetism results

All six Blue Creek Flow paleomagnetic samples exhibit similar demagnetization behavior. A consistent and well-defined characteristic remanent magnetization (ChRM) direction is defined after a weak normal polarity overprint is removed (Fig. 7a). Each analysis clearly indicates a reverse polarity ChRM direction fit by principal component analysis (PCA; Kirschvink, 1980), with a Fisher mean inclination of −77.0° and a mean declination of 167.1° ($\alpha_{95} = 6.8°$, $k = 98.6$; Fig. 7c). The site mean inclination is steeper than the time-averaged dipole inclination at the sampling site, but this discrepancy can be explained straightforwardly by one or both of the following: a) we have assumed that the Blue Creek Flow site has not been tilted since eruption, but it may, in fact require a tilt-correction or b) the flow records a spot reading of the geomagnetic field direction and is not expected to record a time-averaged direction (i.e., the steeper direction is simply recording secular variation of the geomagnetic field). In either case, however, the magnetic polarity recorded by the Blue Creek Flow is unambiguously reversed.

Demagnetization of the eight core specimens of the Headquarters Flow results in a normal polarity direction after a weak – and what we interpret as secondary – viscous overprint is removed. Three specimens require great circle fits (Halls, 1978) to interpret

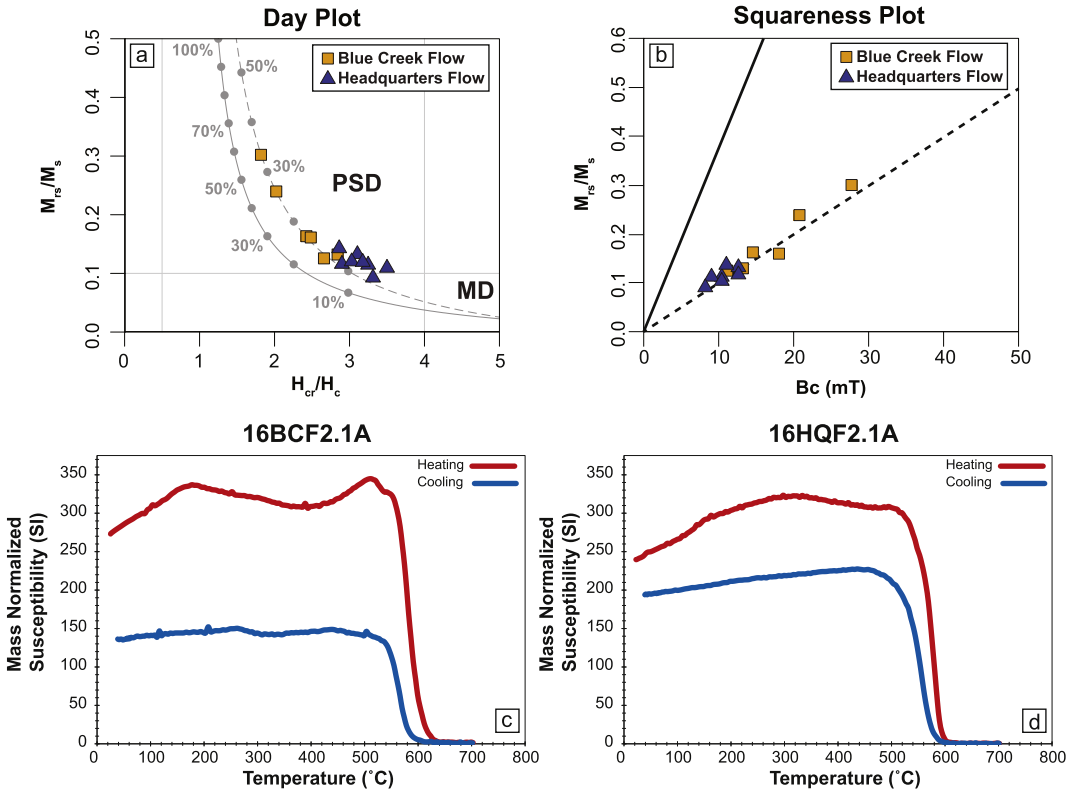

Fig. 6. (a) Day plot of magnetic hysteresis data from Blue Creek (BCF) and Headquarters (HQF) Flows showing the inferred magnetic grain size of bulk specimens and magnetic grain size fields (thin solid gray lines; PSD: pseudosingle-domain; MD: multidomain). Thick solid gray line is a theoretical mixing curve of MD and uniaxial single-domain (SD) magnetite; dashed gray line is a mixing curve of MD and cubic SD magnetite. Points indicate the percentage of SD grains in the mixture (Dunlop, 2002). (b) Squareness plot of BCF and HQF magnetic hysteresis data. The dashed line shows the trend of titanium-poor magnetite, whereas the solid line shows the trendline of young unoxided mid-ocean ridge basalt (titanomagntite of composition TM60). These trendlines are linear regressions of data described by Wang and Van der Voo (2004). (c, d) Magnetic susceptibility versus temperature for BCF (c) and HQF (d). The steep drop near 580 °C in the heating curve indicates a Ti-poor titanomagnetite component.

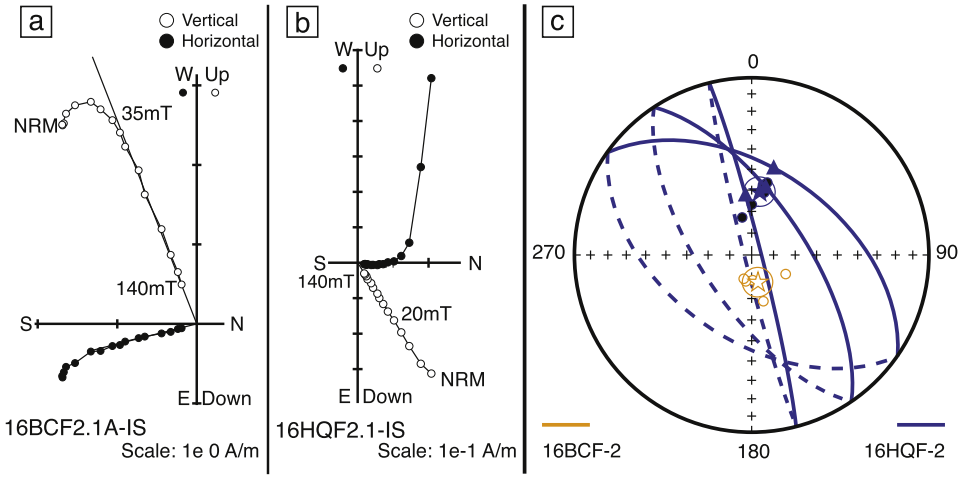

Fig. 7. (a, b) Representative Zijderveld plots for specimens (a) 16BCF-2.1a and (b) 16HQF-2.1a. All Zijderveld diagrams depict the demagnetization of natural remanent magnetization (NRM), following 13–14 alternating field demagnetization treatment steps. Open (closed) circles indicate inclination (declination). (c) Equal angle projection for site mean directions of 16BCF-2 and 16HQF-2. Open (closed) circles indicate upward (downward) pointing inclinations and degree markings along the parameter of the plot indicate declination from geographic north. Star indicates the site mean direction for each site, with the enclosing circles representing the α_{95} uncertainty. Great circles for analyses of 16HQF-2 are indicated by the solid-dashed blue lines ($n = 3$). (For interpretation of the references to color in this figure, the reader is referred to the web version of this article.)

the approximate ChRM direction, whereas the remaining five specimens show univectorial decay of the magnetization toward the origin in Zijderveld plots and therefore can be fit using PCA (see Supplementary Materials). We use the method of McFadden and McElhinny (1988) to combine our great circle and PCA direction fits to calculate a site mean inclination of 60.8° and mean declination of 6.2° ($\alpha_{95} = 7.0°$, $k = 68.4$; Fig. 7c).

4. Interpretations

4.1. Implications for the geomagnetic polarity time scale

Improvement of age determinations using the $^{40}Ar/^{39}Ar$ technique provide an opportunity to evaluate the tempo of eruptions and better constrain geomagnetic polarity excursions. These ages

also resolve discrepancies between field-based stratigraphy and earlier K/Ar ages. We refine the eruption age for the Rhyolite of Snake River Butte to 2.14 Ma. This is consistent with the zircon crystallization ages of 2.15 to 2.17 Ma by Rivera et al. (2014) and Wotzlaw et al. (2015). Previous paleomagnetic data assigned a normal polarity to this unit (Christiansen, 1982). No new paleomagnetic data were obtained on this unit because the eruption age places the unit well within the Reunion subchron (C2r.1n; Gradstein et al., 2004; Hilgen et al., 2012), which has also been called the Feni Drift subchron (Singer, 2014; Singer et al., 2014). Thus, the normal paleomagnetic direction reported by Christiansen (1982) agrees when considering the geochronology and resolves the stratigraphic discrepancy indicated by Obradovich (1992).

Our data remain consistent with the field relationships between the Blue Creek and Headquarters Flows as determined by Christiansen (1982), but significantly improve the accuracy and precision of the eruption ages. Previous K/Ar ages for these two units were indistinguishable from each other. Here, we show that the eruptions took place 30–40 kyr apart, a period of volcanic quiescence previously unrecognized.

Additionally, the age data obtained for the Blue Creek Flow supports earlier U–Pb zircon dating on this unit. Zircon ages determined by ion microprobe range from 3.2 to 1.8 Ma, with a weighted mean age of 1.87 ± 0.09 Ma and a second population with an age of 2.20 ± 0.27 Ma (Bindeman et al., 2001, 2008). The spread of the data, obtained on both crystal cores and rims, led the authors to conclude that significant recycling of earlier formed magmas had occurred, which was also supported by the oxygen isotope values (Bindeman et al., 2008). The sanidine grains analyzed here demonstrate similar recycling: two of the six plateau-forming analyses yield older ages, which may reflect partial resetting of sanidine crystals from the magma that produced the Huckleberry Ridge Tuff.

When our new $^{40}Ar/^{39}Ar$ data are coupled with the new paleomagnetic analyses, the results have important implications. Whereas we confirm the previously determined normal polarity for the Headquarters Flow, we revise that of the Blue Creek Flow. The Blue Creek Flow records a period of reversed polarity at 1.98 Ma, placing it within the Matuyama Chron (C2r.1r). The exceptionally linear paths of demagnetization in Zijderveld projections emphasize the excellent quality of data collected from the Blue Creek Flow, as does the tight clustering of ChRM directions at the site level. The Blue Creek Flow is unambiguously reversed at demagnetization levels >35 mT. That previous results indicated normal polarity (Christiansen, 1982) is likely due to incomplete removal of a normal overprint by low peak cleaning fields; however, since no original data were published, this is our speculation based on our own detailed demagnetization protocol.

Our results, therefore, allow us to add precise temporal constraints to the geomagnetic polarity time scale (GPTS; Fig. 8). First, the eruption age and the unambiguously normal polarity of the Headquarters Flow presents a conflict with a recently proposed age for the onset of the Olduvai subchron. At IODP Site U1308 in the North Atlantic, Channell et al. (2016) suggest that the onset of the Olduvai should be revised to marine oxygen isotope stage (MIS) 73 at 1.925 Ma. However, we identified a fully normally magnetized lava with an age of 1.948 ± 0.004 Ma. Thus, we suggest revision of the GPTS to refine the onset of the Olduvai subchron, recommending that the minimum age for the onset be no younger than 1.948 Ma (but could be slightly older). We recognize that the Headquarters Flow provides only one snapshot of the geomagnetic field at the time of eruption, yet it should be noted that our minimum age of the onset of the Olduvai subchron at 1.948 ± 0.004 Ma is within uncertainty of the astronomical calibrations used in the current version of the GPTS that place the onset

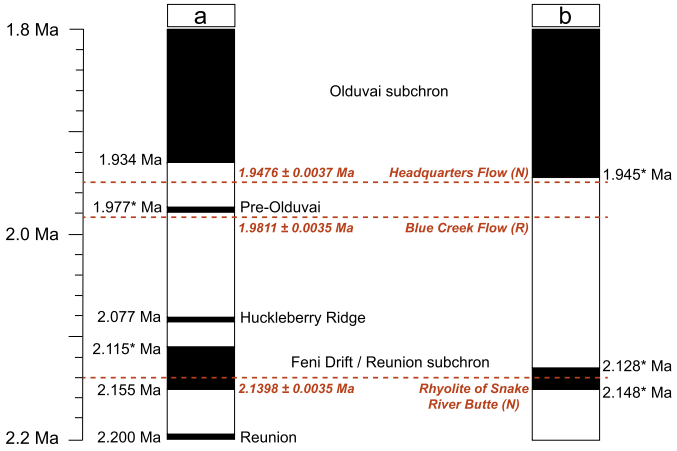

Fig. 8. Portion of the geomagnetic polarity time scale adapted from (a) Singer (2014) and (b) Gradstein et al. (2004) and Hilgen et al. (2012). All ages are calculated relative to the Fish Canyon sanidine standard with an age of 28.201 Ma (Kuiper et al., 2008). Boundary ages marked with an asterisk (*) are derived from astrochronology. $^{40}Ar/^{39}Ar$ ages obtained in this study are indicated by bold, italic, colored font and reported with 2σ full external uncertainties. Normal polarity of an individually dated flow is defined by (N); reversed polarity is indicated by (R). Normal polarity within the time scale is indicated by black; reversed is white.

of the Olduvai subchron (C2n) at 1.945 Ma (Gradstein et al., 2004; Hilgen et al., 2012 and references therein). This boundary has significant implications for hominin migration and evolution, suggesting that fossils from the Turkana Basin, Kenya may be older than originally determined (e.g., Joordens et al., 2013). Therefore, additional work on lavas from this time period should be conducted.

Revision of the polarity of the Blue Creek Flow provides another crucial constraint for the GPTS. The Pre-Olduvai excursion is recorded in ODP Site 983 and 984 sediments, astronomically dated at 1.977 Ma (Channell et al., 2002), and recognized in terrestrial sediments of the Kenyan Turkana Basin (Joordens et al., 2013). Although not specifically identified, the Pre-Olduvai excursion may be represented by a relative paleointensity low, a feature commonly associated with geomagnetic excursions or reversals, ~30 kyr before the onset of the Olduvai subchron in EPAPIS-3Ma (equatorial Pacific paleointensity stack) at ~1.985 in equatorial Pacific sediments (Yamazaki and Oda, 2005). As of this writing, no known lavas record this excursion (Singer, 2014). Reversed polarity at 1.981 ± 0.004 Ma can be interpreted in a number of ways. First, the presence of reversed polarity at ~45°N at this time could indicate that the excursion occurred before or after the eruption of the Blue Creek Flow. Second, if the 1.977 Ma age for the excursion is accurate, then the time offset between the reversed polarity recorded in the Blue Creek Flow and the normal polarity recorded in ODP-recovered sediments could suggest that the onset of the Pre-Olduvai excursion occurred in less than 4000 yrs, which is faster than typically resolved for reversals (Coe and Glen, 2004; Valet et al., 2012), but entirely consistent with some recent observations (Sagnotti et al., 2014, 2016) and geodynamo models (Coe et al., 2000). Given the lack of subaerial lavas and limited number of sedimentary records that record the Pre-Olduvai excursion, the global existence and timing of the Pre-Olduvai remains unresolved. Our work, however, provides a reversed polarity anchor for future GPTS revisions.

4.2. Duration of a super-eruption cycle

Many studies have focused on the intervals between super-eruptions, but relatively few have focused on the duration of a super-eruption cycle. Earlier K/Ar ages of these Yellowstone units suggested that the duration of the first-cycle volcanism occurred over a 400 kyr period (from 2.2 to 1.8 Ma; Obradovich, 1992).

Table 2
Duration of quiescence between each of the Yellowstone Volcanic Field first cycle eruptions and total duration of the first eruption cycle.

Units	Quiescence duration (Ma)
Headquarters Flow to Blue Creek Flow	0.0335 ± 0.0051
Blue Creek Flow to Huckleberry Ridge Tuff	0.0961 ± 0.0054
Huckleberry Ridge Tuff to Rhyolite of Snake River Butte	0.0626 ± 0.0054
	Total duration (Ma)
Headquarters Flow to Rhyolite of Snake River Butte	0.1922 ± 0.0051

Improvements in the $^{40}Ar/^{39}Ar$ technique have reduced this duration to approximately 200 kyr (from 2.14 to 1.95 Ma; Table 2). Additionally, the high-precision $^{40}Ar/^{39}Ar$ dates for these lavas indicate that volcanism is punctuated within the Yellowstone Volcanic Field. The Blue Creek Flow was the first eruption following evacuation of the Huckleberry Ridge magma chamber and occurred ~100 kyr after the super-eruption. The Headquarters Flow then erupted ~40 kyr later. This sequence of events places tight constraints on the residence time for post-supereruption magmas. Smaller volume magmas, such as these, may either be produced by rejuvenation of a pre-existing magma body, or by separate, isolated magma batches. Chemical and isotopic analyses would allow for determining the source of the magma and whether it is stored 'warm' or 'cold' (Barboni et al., 2016; Cooper and Kent, 2014), but these analyses are beyond the scope of this paper. Rather, we rely on the $^{40}Ar/^{39}Ar$ eruption ages of these units to define the periodicity of eruptions. We conclude that magmatic residence is on timescales <40 kyr.

Punctuated volcanism within the Yellowstone Volcanic Field has also been identified in the lavas that surfaced between the Mesa Falls and Lava Creek caldera-forming eruptions. New $^{40}Ar/^{39}Ar$ eruption ages for the Island Park and Mount Jackson (IPMJ) Rhyolites led Troch et al. (2017) to identify a similar period of quiescence between intra-caldera and caldera-forming eruptions. However, in examining the IPMJ lavas, Troch et al. (2017) found periods of quiescence as long as 290 kyr – nearly three times as long as the longest period of inactivity determined by our studies. Troch et al. (2017) note that this long duration may be an artefact of an incomplete record: subsequent super-eruptions could destroy lavas that surfaced within this perceived period of quiescence. We note that prior to the most recent period of volcanism within the active Yellowstone caldera, the magmatic system appears to have been quiescent for ~220 kyr and that the period of quiescence since the last Yellowstone super-eruption is ~75 kyr (e.g., Stelten et al., 2015).

Our results provide a minimum duration for the first eruption cycle of the Yellowstone Volcanic Field of approximately 200 kyr. Second cycle volcanism, which includes three eruptions prior to the eruption of the Mesa Falls Tuff (Green Canyon Flow, Bishop Mountain Flow, and the Tuff of Lyle Spring) and the Island Park Rhyolites, spans an interval of ~240 kyr (Furlong et al., 2016; Gardiner et al., 2016; Troch et al., 2017; Vincent et al., 2016). Third cycle volcanism, consisting of flows erupted before and after the formation of the Yellowstone Caldera (Mount Jackson Rhyolites, Lava Creek Tuff, and Plateau Rhyolites), span an interval of >700 kyr. Pre-caldera eruptions began some 200 kyr prior to the super-eruption producing the Lava Creek Tuff (Troch et al., 2017; Matthews et al., 2015; Rivera and Jicha, 2015), and post-caldera eruptions are as young as 75 kyr (Stelten et al., 2015). This begs the question: Is the duration of super-eruption cycles becoming longer?

Given the unique tectonic setting and pattern of magmatism found in the Yellowstone Volcanic Field and surrounding Snake River Plain, analogous caldera-forming systems are few. For example, the Long Valley caldera system has pre-eruptive effusive rhyolites, but only one known caldera. The Taupo region also has a long volcanic history, but the magmas are more compositionally diverse and have been influenced by slab-derived fluids (e.g., Cole et al., 2014; Deering et al., 2011), unlike the compositional homogeneity exhibited by the caldera-forming and effusive magmas at Yellowstone (Christiansen, 2001). However, the Jemez Volcanic Field in New Mexico may be suitable for comparison because there have been at least two caldera forming eruptions and many post-caldera effusive rhyolites. Although this system is intracontinental, magmatism is driven by extensional forces rather than a presumed hotspot like that suggested for the Yellowstone region.

The Valles Caldera was produced from eruption of the Upper Bandelier Tuff at 1.264 ± 0.010 Ma and post-caldera high-silica rhyolites erupted from the time of caldera formation until 1.216 ± 0.017 Ma (Zimmerer et al., 2016, and references therein), for a duration of ~50 kyr. Following the eruption of the post-caldera rhyolites at ~1.2 Ma, there was volcanic quiescence for approximately 200 kyr and flare-ups continued to occur every ~200 kyr until the eruption of South Mountain at 527 ± 4 kyr (Zimmerer et al., 2016). Volcanic activity then ceased for some 400 kyr, until the East Fork Member eruptions began. These eruptions are chemically and mineralogically distinct from the Valles Caldera rhyolites, and have been interpreted to signify the beginning of a new volcanic cycle (Zimmerer et al., 2016). Therefore, in the Bandelier system, the available age data suggest that the duration of the Valles Caldera cycle is at least 50 kyr and may be as long as 200 kyr, similar to the duration observed in the Yellowstone Volcanic Field. Although the tectonic setting, magmatic processes, and chemical signatures are different in the two areas, timescales of volcanic activity within the interior west of North America may be on the same order.

5. Conclusions

The improved analytical techniques for $^{40}Ar/^{39}Ar$ dating over the last decade provide opportunities to examine the tempo of Pleistocene volcanism within the Yellowstone Volcanic Field with unprecedented accuracy and precision, thus providing insights into magma residence and recharge and holistic views on periodicities of quiescence and activity. This work provides the first high-precision $^{40}Ar/^{39}Ar$ dates for the effusive eruptions bounding the caldera-forming eruption that produced the Huckleberry Ridge Tuff. The improved eruption age for the Rhyolite of Snake River Butte resolves the previously enigmatic stratigraphic inconsistency between this and the Huckleberry Ridge Tuff. Additionally, our new dates for the Blue Creek and Headquarters Flows led to the discovery of a new period of volcanic quiescence within the broader super-eruption cycle. The timing of eruptions following caldera formation place constraints on the duration of magmatic residence, limiting this time period to no more than 40 kyr. Furthermore, our results demonstrate that the duration of the first volcanic cycle of the Yellowstone Volcanic Field can be reduced from 400 kyr to 200 kyr. An analysis of the eruption ages for the small-volume rhyolites and caldera-forming eruptions in the Jemez Volcanic Field suggests a similar duration of volcanic activity (50 kyr to 200 kyr), which may suggest that caldera-forming systems in the intermountain west of the United States operate on similar timescales, albeit in different tectonic environments.

These dates are supplemented with a comprehensive analysis of rock magnetic and paleomagnetic characteristics of the lavas. We determined that the polarity of the Blue Creek Flow is reversed, in contrast to previously reported reconnaissance-level paleomagnetic studies. Our $^{40}Ar/^{39}Ar$ eruption ages and paleomagnetic results constrain the minimum age for the onset of the Olduvai subchron

of the geomagnetic polarity time scale to 1.948 Ma and provide a reversed-polarity constraint (of 1.981 Ma) preceding the Pre-Olduvai excursion. These ages are particularly useful as markers within the history of human evolution, but we suggest additional work on lavas from this time period to test and better constrain the timing of these geomagnetic reversal boundaries.

Acknowledgements

The authors would like to thank Ilya Bindeman, two anonymous reviewers, and editor Tamsin Mather for helpful comments to improve this manuscript. Full processed data can be found online in the Supplementary Materials. This research was funded by a grant from the National Science Foundation (NSF) Earth Sciences Division (EAR) Petrology and Geochemistry Program (EAR-1524840 to TR and EAR-1524825 to MS). Field and/or lab assistance was provided by R. Furlong, S. Gardiner, V. Isakson, A. Laib, and J. Vincent.

Appendix A. Supplementary material

Supplementary material related to this article can be found online at http://dx.doi.org/10.1016/j.epsl.2017.08.027.

References

Barboni, M., Boehnke, P., Schmitt, A.K., Harrison, T.M., Shane, P., Bouvier, A.-S., Baumgartner, L., 2016. Warm storage for arc magmas. Proc. Natl. Acad. Sci. 113, 13959–13964. http://dx.doi.org/10.1073/pnas.1616129113.

Bindeman, I.N., Valley, J.W., Wooden, J.L., Persing, H.M., 2001. Post-caldera volcanism: in situ measurement of U–Pb age and oxygen isotope ratio in Pleistocene zircons from Yellowstone caldera. Earth Planet. Sci. Lett. 189, 197–206.

Bindeman, I.N., Fu, B., Kita, N.T., Valley, J.W., 2008. Origin and evolution of silicic magmatism at Yellowstone based on ion microprobe analysis of isotopically zoned zircons. J. Petrol. 49, 163–193.

Bindeman, I.N., Simakin, A.G., 2014. Rhyolites—hard to produce, but easy to recycle and sequester: integrating microgeochemical observations and numerical models. Geosphere 10, 930.

Channell, J.E.T., Mazaud, A., Sullivan, P., Turner, S., Raymo, M.E., 2002. Geomagnetic excursions and paleointensities in the Matuyama Chron at Ocean Drilling Program Sites 983 and 984 (Iceland Basin). J. Geophys. Res. 107 (B6).

Channell, J.E.T., Labs, J., Raymo, M.E., 2003. The réunion subchronozone at ODP site 981 (Feni Drift, North Atlantic). Earth Planet. Sci. Lett. 215, 1–12.

Channell, J.E.T., Hodell, D.A., Curtis, J.H., 2016. Relative paleointensity (RPI) and oxygen isotope stratigraphy at IODP Site U1308: North Atlantic RPI stack for 1.2–2.2 Ma (NARPI-2200) and age of the Olduvai Subchron. Quat. Sci. Rev. 131, 1–19.

Christiansen, R.L., 1982. Late Cenozoic volcanism of the Island Park area, eastern Idaho. In: Bonnichsen, B., Breckenridge, R.M. (Eds.), Cenozoic Geology of Idaho. Idaho Bureau of Mines and Geology Bulletin, pp. 345–368.

Christiansen, R.L., 2001. The Quaternary and Pliocene Yellowstone Plateau Volcanic Field of Wyoming, Idaho, and Montana. United States Geological Survey Professional Paper 729-G.

Christiansen, R.L., Blank, J., Richard, H., 1972. Volcanic stratigraphy of the Quaternary rhyolite plateau in Yellowstone National Park. United States Geological Survey Professional Paper 729-B.

Coe, R.S., Glen, J.M.G., 2004. The complexity of reversals. In: Channell, J.E.T., Kent, D.V., Lowrie, W., Meert, J. (Eds.), Timescales of the Paleomagnetic Field: American Geophysical Monograph, vol. 145. American Geophysical Union, Washington, D.C., pp. 1–12.

Coe, R.S., Hongre, L., Glatzmaier, G.A., 2000. An examination of simulated geomagnetic reversals from a paleomagnetic perspective. Philos. Trans. R. Soc. Lond. Ser. A, 1141–11870.

Cole, J.W., Deering, C.D., Burt, R.M., Sewell, S., Shane, P.A.R., Matthews, N.E., 2014. Okataina Volcanic Centre, Taupo Volcanic Zone, New Zealand: a review of volcanism and synchronous pluton development in an active, dominantly silicic caldera system. Earth-Sci. Rev. 128, 1–17.

Cooper, K.M., Kent, A.J., 2014. Rapid remobilization of magmatic crystals kept in cold storage. Nature 506, 480–483.

Day, R., Fuller, M., Schmidt, V.A., 1977. Hysteresis properties of titanomagnetites: grain size and composition dependence. Phys. Earth Planet. Inter. 13, 260–267.

Deering, C.D., Bachmann, O., Dufek, J., Gravley, D.M., 2011. Rift-related transition from andesite to rhyolite volcanism in the Taupo Volcanic Zone (New Zealand) controlled by crystal-melt dynamics in mush zones with variable mineral assemblages. J. Petrol. 52, 2243–2263.

Dunlop, D.J., 2002. Theory and application of the Day plot (Mrs/Ms versus Hcr/Hc) 1. Theoretical curves and tests using titanomagnetite data. J. Geophys. Res., Solid Earth 107 (B3). http://dx.doi.org/10.1029/2001JB000486.

Ellis, B.S., Mark, D.F., Troch, J., Bachmann, O., Guillong, M., Kent, A.J.R., von Quadt, A., 2017. Split-grain $^{40}Ar/^{39}Ar$ dating: integrating temporal and geochemical data from crystal cargoes. Chem. Geol. 457, 15–23.

Fleck, R.J., Sutter, J.F., Elliot, D.H., 1977. Interpretation of discordant $^{40}Ar/^{39}Ar$ age-spectra of Mesozoic tholeiites from Antarctica. Geochim. Cosmochim. Acta 41 (1), 15–32.

Furlong, R., Rivera, T.A., Lippert, P.C., Jicha, B.R., Schmitz, M.D., 2016. New $^{40}Ar/^{39}Ar$ and paleomagnetic data from the Bishop Mountain Flow, Yellowstone Volcanic Field. Abstr. Program – Geol. Soc. Am. 48 (7).

Gardiner, S., Rivera, T.A., Jicha, B.R., Schmitz, M.D., 2016. New $^{40}Ar/^{39}Ar$ sanidine dates and zircon imaging for the Green Canyon Flow, Yellowstone Volcanic Field. Abstr. Program – Geol. Soc. Am. 48 (7).

Gradstein, F.M., Ogg, J.G., Smith, A., 2004. A Geologic Time Scale 2004. Cambridge University Press.

Gradstein, F.M., Ogg, J.G., Schmitz, M.D., Ogg, G.M., 2012. The Geologic Time Scale 2012. Elsevier.

Gee, J., Kent, D.V., 1995. Magnetic hysteresis in young mid-ocean ridge basalts: dominant cubic anisotropy? Geophys. Res. Lett. 22, 551–554.

Halls, H.C., 1978. The use of converging remagnetization circles in paleomagnetism. Phys. Earth Planet. Inter. 16, 1–11.

Hilgen, F.J., Lourens, L.J., Van Dam, J.A., 2012. The Neogene period. In: Gradstein, F.M., Ogg, J.G., Schmitz, M.D., Ogg, G. (Eds.), The Geologic Time Scale 2012. Elsevier, Amsterdam, pp. 923–978.

Jicha, B.R., Singer, B.S., Sobol, P., 2016. Re-evaluation of the ages of $^{40}Ar/^{39}Ar$ sanidine standards and supereruptions in the western U.S. using a Noblesse multi-collector mass spectrometer. Chem. Geol. 431, 54–66.

Joordens, J.C., Dupont-Nivet, G., Feibel, C.S., Spoor, F., Sier, M.J., van der Lubbe, J.H., Nielsen, T.K., Knul, M.V., Davies, G.R., Vonhof, H.B., 2013. Improved age control on early Homo fossils from the upper Burgi Member at Koobi Fora, Kenya. J. Hum. Evol. 65, 731–745.

Kirschvink, J.L., 1980. The least-square line and plane and the analysis of paleomagnetic data. Geophys. J. R. Astron. Soc. 62, 699–718.

Kuiper, K.F., Deino, A., Hilgen, F.J., Krijgsman, W., Renne, P.R., Wijbrans, J.R., 2008. Synchronizing rock clocks of Earth history. Science 320, 500–504.

Matthews, N.E., Vazquez, J.A., Calvert, A., 2015. Age of the Lava Creek supereruption and magma chamber assembly at Yellowstone based on $^{40}Ar/^{39}Ar$ and U–Pb dating of sanidine and zircon crystals. Geochem. Geophys. Geosyst.. http://dx.doi.org/10.1002/2015GC005881.

McFadden, P.L., McElhinny, M.W., 1988. The combined analysis of remagnetization circles and direct observations in paleomagnetism. Earth Planet. Sci. Lett. 87, 161–172.

Min, K., Mundil, R., Renne, P.R., Ludwig, K.R., 2000. A test for systematic errors in $^{40}Ar/^{39}Ar$ geochronology through comparison with U/Pb analysis of a 1.1-Ga rhyolite. Geochim. Cosmochim. Acta 64, 73–98. http://dx.doi.org/10.1016/S0016-7037(99)00204-5.

Obradovich, J.D., 1992. Geochronology of the Late Cenozoic Volcanism of Yellowstone National Park and Adjoining Areas, Wyoming and Idaho. U.S. Geological Survey.

Reynolds, R.L., 1977. Paleomagnetism of welded tuffs of the Yellowstone Group. J. Geophys. Res. 82, 3677–3693. http://dx.doi.org/10.1029/JB082i026p03677.

Rivera, T.A., Jicha, B.R., 2015. $^{40}Ar/^{39}Ar$ single crystal sanidine dates for the Lava Creek Tuff (member B). Integrated Earth Data Applications (IEDA). http://dx.doi.org/10.1594/IEDA/100549.

Rivera, T.A., Schmitz, M.D., Crowley, J.L., Storey, M., 2014. Rapid magma evolution constrained by zircon petrochronology and $^{40}Ar/^{39}Ar$ sanidine ages for the Huckleberry Ridge Tuff, Yellowstone, USA. Geology 42, 643–646. http://dx.doi.org/10.1130/g35808.1.

Rivera, T.A., Schmitz, M.D., Jicha, B.R., Crowley, J.L., 2016. Zircon petrochronology and $^{40}Ar/^{39}Ar$ sanidine dates for the Mesa Falls Tuff: crystal-scale records of magmatic evolution and the short lifespan of a large Yellowstone magma chamber. J. Petrol. 57, 1677–1704. http://dx.doi.org/10.1093/petrology/egw053.

Rivera, T.A., Storey, M., Schmitz, M.D., Crowley, J.L., 2013. Age intercalibration of $^{40}Ar/^{39}Ar$ sanidine and chemically distinct U/Pb zircon populations from the Alder Creek Rhyolite Quaternary geochronology standard. Chem. Geol. 345, 87–98. http://dx.doi.org/10.1016/j.chemgeo.2013.02.021.

Sagnotti, L., Scardia, G., Giaccio, B., Liddicoat, J.C., Nomade, S., Renne, P.R., Sprain, C.J., 2014. Extremely rapid directional change during Matuyama-Brunhes geomagnetic polarity reversal. Geophys. J. Int. 199, 1110–1124. http://dx.doi.org/10.1093/gji/ggu287.

Sagnotti, L., Giaccio, B., Liddicoat, J.C., Nomade, S., Renne, P.R., Scardia, G., Sprain, C.J., 2016. How fast was the Matuyama–Brunhes geomagnetic reversal? A new subcentennial record from the Sulmona Basin, central Italy. Geophys. J. Int. 204, 798–812. http://dx.doi.org/10.1093/gji/ggv486.

Singer, B.S., 2014. A Quaternary geomagnetic instability time scale. Quat. Geochronol. 21, 29–52. http://dx.doi.org/10.1016/j.quageo.2013.10.003.

Singer, B.S., Jicha, B.R., Condon, D.J., Macho, A.S., Hoffman, K.A., Dierkhising, J., Brown, M.C., Feinberg, J.M., Kidane, T., 2014. Precise ages of the Réunion event and Huckleberry Ridge excursion: episodic clustering of geomagnetic instabilities and the dynamics of flow within the outer core. Earth Planet. Sci. Lett. 405, 25–38. http://dx.doi.org/10.1016/j.epsl.2014.08.011.

Stelten, M.E., Cooper, K.M., Vazquez, J.A., Calvert, A.T., Glessner, J.J.G., 2015. Mechanisms and timescales of generating eruptible rhyolitic magmas at Yellowstone Caldera from zircon and sanidine geochronology and geochemistry. J. Petrol. 56, 1607–1642.

Troch, J., Ellis, B.S., Mark, D.F., Bindeman, I.N., Kent, A.J.R., Guillong, M., Bachmann, O., 2017. Rhyolite generation prior to a Yellowstone supereruption: insights from the Island Park–Mount Jackson rhyolite series. J. Petrol. egw071.

Valet, J.-P., Fournier, A., Courtillot, V., Herrero-Bervera, E., 2012. Dynamical similarity of geomagnetic field reversals. Nature 490, 89–93. http://dx.doi.org/10.1038/nature11491.

Vincent, J., Rivera, T.A., Jicha, B.R., Lippert, P.C., Schmitz, M.D., 2016. Lithology of the tuff of Lyle Spring, Yellowstone volcanic field. Abstr. Program – Geol. Soc. Am. 48 (7).

Wang, D., Van der Voo, R., 2004. The hysteresis properties of multidomain magnetite and titanomagnetite/titanomaghemite in mid-ocean ridge basalts. Earth Planet. Sci. Lett. 220, 175–184. http://dx.doi.org/10.1016/S0012-821X(04)00052-4.

Wotzlaw, J.F., Bindeman, I.N., Stern, R.A., D'Abzac, F.X., Schaltegger, U., 2015. Rapid heterogeneous assembly of multiple magma reservoirs prior to Yellowstone supereruptions. Sci. Rep. 5, 14026. http://dx.doi.org/10.1038/srep14026.

Yamazaki, T., Oda, H., 2005. A geomagnetic paleointensity stack between 0.8 and 3.0 Ma from equatorial Pacific sediment cores. Geochem. Geophys. Geosyst. 6. http://dx.doi.org/10.1029/2005gc001001.

Zimmerer, M.J., Lafferty, J., Coble, M.A., 2016. The eruptive and magmatic history of the youngest pulse of volcanism at the Valles caldera: implications for successfully dating late Quaternary eruptions. J. Volcanol. Geotherm. Res. 310, 50–57.